

'Pink'-beam X-ray powder diffraction profile and its use in Rietveld refinement

Robert B. Von Dreele,^{a*} Samantha M. Clarke^b and James P. S. Walsh^c

^aArgonne National Laboratory, 9700 South Cass Avenue, Lemont, IL 60439-4814, USA, ^bLawrence Livermore National Laboratory, 7000 East Avenue, Livermore, CA 94550, USA, and ^cDepartment of Chemistry, University of Massachusetts Amherst, Amherst, MA 01003, USA. *Correspondence e-mail: vondreele@anl.gov

Received 12 August 2020

Accepted 4 November 2020

Edited by H. Brand, Australian Synchrotron, Australia

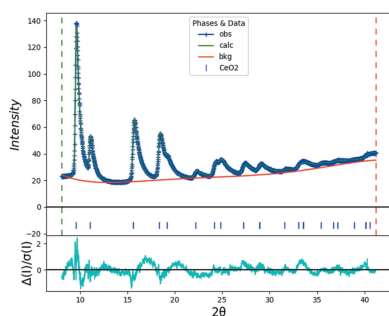
Keywords: powder diffraction; pink beams; Rietveld refinement.

The powder diffraction profile obtained with a pink-beam synchrotron X-ray source is described as the convolution of a back-to-back pair of exponentials convoluted with the Gaussian and Lorentzian components of a pseudo-Voigt. This new function is employed for the first time in a Rietveld refinement using data collected from a single 100 ps synchrotron X-ray micropulse.

1. Introduction

The Laser Shock Station (LSS) is part of the Dynamic Compression Sector (DCS) at the Advanced Photon Source (APS) and provides laser-driven shock compression linked to high-energy X-ray pulses from the APS at Sector 35 to realize *in situ* time-resolved X-ray diffraction patterns of materials under well characterized shock conditions (Wang *et al.*, 2019). Prior to *in situ* X-ray diffraction, identification of phase transitions in shock-loaded samples had been inferred from the correlation between shock-wave-profile analyses and previously identified static high-pressure structural information (Bancroft *et al.*, 1956). The advance of ultrafast diffraction probes such as at the LSS has enabled numerous discoveries, including revealing previously unknown phase transitions in elements that were thought to be well understood, such as gold (Briggs *et al.*, 2019) and silver (Sharma *et al.*, 2020). The discovery of these new high-pressure phases emphasizes the importance of implementing X-ray diffraction techniques to directly study the structure of materials under shock compression rather than relying on shock-wave-profile analysis, which can fail to capture phase transitions with small volume changes.

The X-ray source is a revolver-type undulator with two period choices. One is the U17 undulator dedicated to 23 keV operation which is the source used in this study. Owing to the inherently short timescale of the experiment, with laser drive pulses being 5–10 ns, *in situ* diffraction experiments of the transient shocked or release state must use single X-ray pulses that have very narrow temporal widths. A single ~100 ps X-ray 'superbunch' micropulse generated in hybrid singlet mode at the APS is well suited for such experiments (Wang *et al.*, 2019). To obtain a sufficiently high photon flux to produce a useful diffraction image at this timescale, the micropulse is then focused and shaped via mirrors and filters to give a quasi-monochromatic 40 μm beam with a bandwidth of 2–5% depending on undulator settings and the white-beam slit size. Fig. 1 shows the shape of this energy profile with a 3.7% bandwidth as $\log(I)$ versus energy; the peak intensity is at 23.676 keV ($\lambda = 0.52368 \text{ \AA}$). Clearly, the intensity profile can



be approximated by a pair of back-to-back exponentials which are then convoluted with a smoothing function (e.g. Gaussian).

To collect powder diffraction data, a Rayonix SX165 detector is positioned 94 mm from the sample position. Fig. 2 shows a powder diffraction image from a single APS micropulse ($\sim 5 \times 10^9$ photons) collected from the NIST standard reference material SRM674b (CeO_2) held in a thin layer between Kapton tapes. An integration of this image gives a one-dimensional powder pattern (Fig. 3) that exhibits a very strong asymmetry of the Bragg peaks. This peak shape strongly resembles that obtained in spallation neutron source time-of-flight (TOF) powder diffraction experiments (Von

Dreele *et al.*, 1982). While most Rietveld (1969) refinement software is capable of modelling data with asymmetric peak shapes that can be approximated using convolutions of simple Lorentzian and Gaussian terms, such approaches prove to be inadequate for fitting patterns with the extremely asymmetric peak shapes obtained with pink-beam methods. For this reason, previous reports from LSS experiments analysed the data by producing simulated X-ray diffraction line profiles of varied lattice parameters to visually match peak position (Sharma *et al.*, 2020) or employed single-peak fits using an exponential–Gaussian convolution (‘Exp–Gauss’) function (Briggs *et al.*, 2019) of the X-ray diffraction patterns rather than true Rietveld refinements. Although the Exp–Gauss function only represents the long tail component of this peak profile, it is acceptable for simple elemental face- and body-centred-cubic structures, but it becomes problematic when the crystal structure is lower symmetry and peak overlap occurs.

Implementing a peak shape function that can allow for a robust full pattern analysis is therefore crucial for the reliable extraction of crystal structure information from diffraction data collected at extreme pressures. Furthermore, the ability to perform quantitative evaluation of phenomena that manifest in subtle ways in diffraction data – such as line broadening caused by strain or intensity differences caused by preferred orientation – will enable much more detailed studies of these exotic states of matter. To this end, we have adapted the neutron TOF peak shape function to pink-beam data and implemented it in the *GSAS-II* Rietveld refinement code (Toby & Von Dreele, 2013). This paper covers the mathematical details of this function and a first application in the Rietveld refinement of CeO_2 .

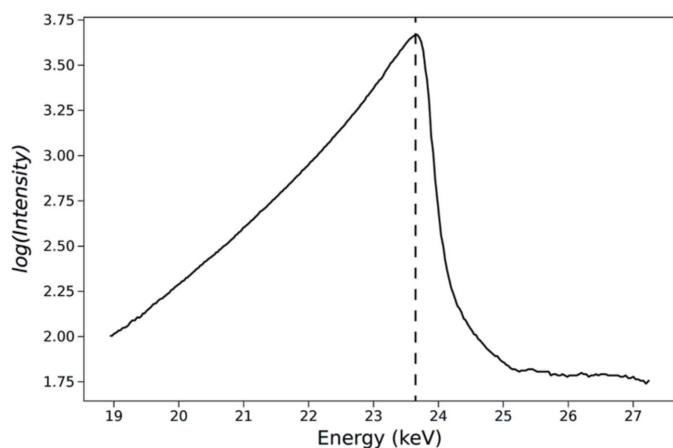


Figure 1 Energy spectrum from the U17 undulator of the Dynamic Compression Sector, Advanced Photon Source, showing the near-exponential intensity rise and decay. Maximum intensity is at 23.68 keV ($\lambda = 0.52368 \text{ \AA}$); bandwidth = 3.7%.

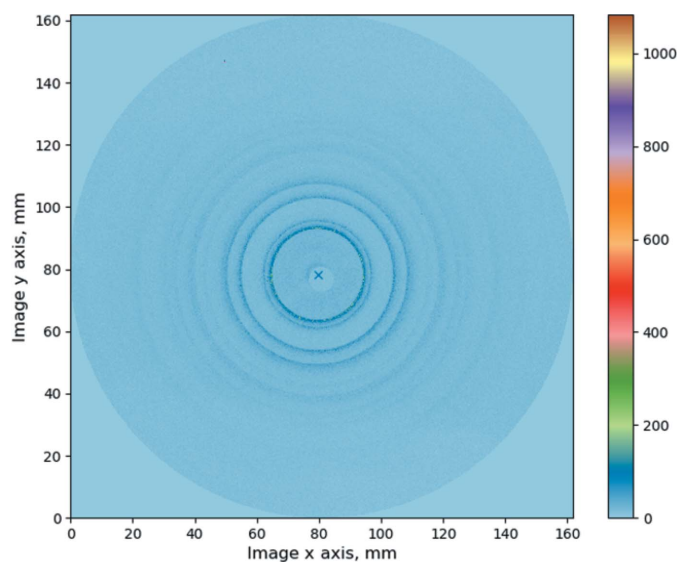


Figure 2 2D powder diffraction pattern of CeO_2 taken on the Laser Shock Station at the Dynamic Compression Sector, Advanced Photon Source, from a single 100 ps photon micropulse collected on a Rayonix XM165 detector 94 mm from sample; the nominal wavelength was 0.5243 \AA .

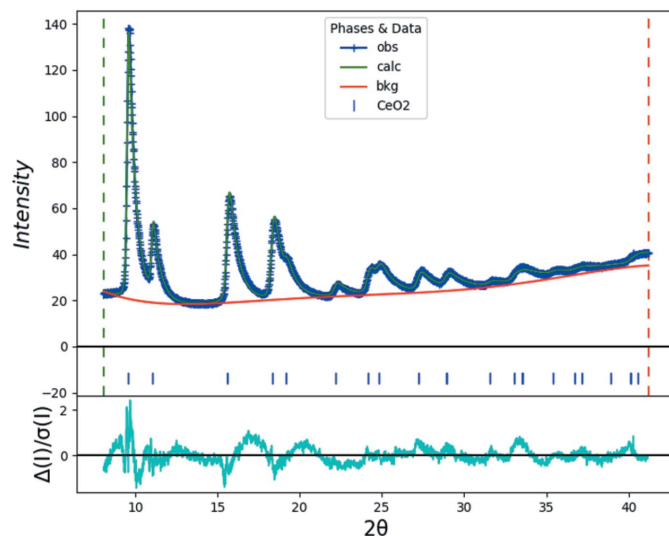


Figure 3 Powder diffraction pattern of CeO_2 taken on the Laser Shock Station at the Dynamic Compression Sector, Advanced Photon Source, integrated from the image collected on a Rayonix XM165 detector with as-calibrated distance 87.73 mm from sample. Also shown is the result of a Rietveld refinement with pink-beam powder diffraction data for CeO_2 ; $R_{wp} = 2.08\%$.

2. The pink-beam powder profile function

To obtain the pink peak shape function, we begin with an approximation to the energy pulse shape (Fig. 1) as a pair of normalized back-to-back exponential functions:

$$\begin{aligned} E(\tau) &= \frac{\alpha\beta}{\alpha + \beta} \exp(\alpha\tau) \quad \tau < 0, \\ E(\tau) &= \frac{\alpha\beta}{\alpha + \beta} \exp(-\beta\tau) \quad \tau > 0. \end{aligned} \quad (1)$$

The intersection ($\tau = 0$) is at the peak in this distribution. To provide the instrumental and possible sample broadening, this distribution is convoluted with both Gaussian and Lorentzian functions. These are then combined via the pseudo-Voigt approximation (Thompson *et al.*, 1987). For the Gaussian component, the convolution yields

$$G(\Delta 2\theta) = \frac{\alpha\beta}{2(\alpha + \beta)} \exp(u) \operatorname{erfc}(y) + \exp(v) \operatorname{erfc}(z), \quad (2)$$

where erfc is the complementary error function and

$$\begin{aligned} u &= \frac{\alpha}{2} (\alpha\sigma^2 + 2\Delta 2\theta), & v &= \frac{\beta}{2} (\beta\sigma^2 - 2\Delta 2\theta), \\ y &= \frac{\alpha\sigma^2 + \Delta 2\theta}{(2\sigma^2)^{1/2}}, & z &= \frac{\beta\sigma^2 - 2\Delta 2\theta}{(2\sigma^2)^{1/2}}, \end{aligned} \quad (3)$$

while for the Lorentzian component the result is

$$L(\Delta 2\theta) = \frac{\alpha\beta}{\pi(\alpha + \beta)} \{ \operatorname{Im}[\exp(p)E_1(p)] + \operatorname{Im}[\exp(q)E_1(q)] \}, \quad (4)$$

where Im is the imaginary part, E_1 is the exponential integral function and

$$p = -\alpha\Delta 2\theta + i\alpha\gamma/2 \quad \text{and} \quad q = -\beta\Delta 2\theta + i\beta\gamma/2. \quad (5)$$

The pseudo-Voigt approximation then gives the overall profile function

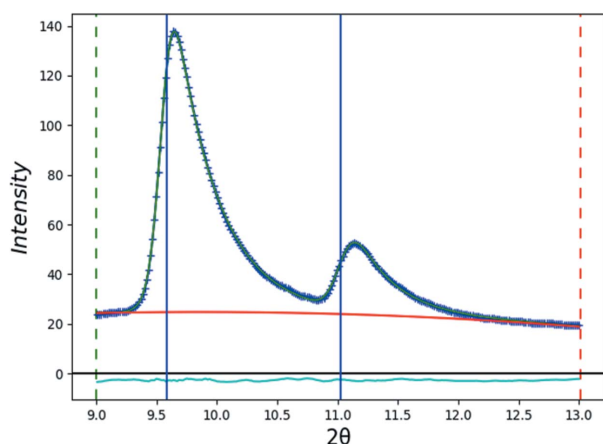


Figure 4
Single-peak fits for the first two reflections in the pink-beam CeO_2 pattern. Vertical blue lines are refined peak positions, the blue curve is the observed data and the green curve is the calculated fit; the background (red) and difference (cyan) are also shown.

$$P(\Delta 2\theta) = \eta L(\Delta 2\theta) + (1 - \eta)G(\Delta 2\theta). \quad (6)$$

The mixing coefficient (η) is defined according to the formulation of Thompson *et al.* (1987) to make the pseudo-Voigt a close approximation to the true Voigt. Thus this function requires the rise and fall exponential coefficients (α and β) and the Gaussian and Lorentzian coefficients (σ and γ) along with position and intensity; it is identical to that used for spallation neutron TOF data with the scattering angle (2θ) in degrees as the independent variable instead of neutron TOF in microseconds.

The success of this function can be seen in Fig. 4, which shows the essentially perfect fit to the first two peaks in the CeO_2 pattern. Note that the peak positions do not coincide with the peak maxima; this is a consequence of the underlying asymmetry of the pink-beam energy profile.

3. Pink-beam Rietveld refinement

In a Rietveld refinement application, the variation of the various peak shape parameters with respect to the independent variable (in this case 2θ) must be established. Because the instrument setup and the method for collecting the pink-beam data are the same as for a conventional constant-wavelength powder diffractometer (*e.g.* beamline 17BM at the APS), it is expected that the Gaussian broadening will follow the formalism originally introduced by Rietveld (1969),

$$\sigma^2 = U \tan^2 \theta + V \tan \theta + W, \quad (7)$$

and that the Lorentzian broadening will follow

$$\gamma = \frac{X}{\cos \theta} + Y \tan \theta, \quad (8)$$

for which the two terms accommodate potential sample crystallite size and microstrain broadening, respectively. For the convenience of comparing the coefficients to ones obtained on conventional instruments, the UVW coefficients are scaled by 10^4 and the XY coefficients are scaled by 100 within *GSAS-II*; this makes the units for these parameters centidegrees squared and centidegrees, respectively. These terms are then further modified by the corresponding crystallite size and powder microstrain parameterization within *GSAS-II*, permitting potential extraction of these data from a Rietveld refinement.

As it is anticipated that the exponential coefficients, α and β , for the pink-beam energy profile should show an increased dispersion with scattering angle, we have adopted the following relations for them:

$$\alpha = \alpha_0 + \alpha_1 \tan \theta \quad (9)$$

and

$$\beta = \beta_0 + \beta_1 \tan \theta. \quad (10)$$

With these functions implemented in *GSAS-II*, a Rietveld refinement of the CeO_2 pattern gives an excellent fit (Fig. 3), allowing a full characterization of the above coefficients.

Table 1

Pink-beam powder diffraction profile coefficients obtained from Rietveld refinement with single micropulse data from NIST SRM 674b CeO₂ at the LSS station of the DCS sector of the APS.

| | |
|------------------------|-------------|
| Wavelength, Å | 0.52015 (4) |
| $U, 10^{4\sigma^2}$ | 0 |
| $V, 10^{4\sigma^2}$ | 0 1021 (55) |
| $W, 10^{4\sigma^2}$ | -69 (5) |
| $X, 10^{2\sigma}$ | 0 |
| $Y, 10^{2\sigma}$ | 56.7 (33) |
| $\alpha_0, ^{\circ-1}$ | 14.4 (5) |
| $\alpha_1, ^{\circ-1}$ | 0 |
| $\beta_0, ^{\circ-1}$ | 3.016 (20) |
| $\beta_1, ^{\circ-1}$ | -7.94 (11) |

4. Discussion

The shape of the pink-beam powder diffraction peaks poses some unique challenges for data processing. Since the data are obtained here as a two-dimensional image from the Rayonix SX165 detector, a calibration step is needed to establish the detector position and orientation before the image can be integrated to produce a one-dimensional powder pattern. Software designed to achieve this (*e.g.* *GSAS-II*) fits a succession of diffraction ring maxima found in the image and assumes that the ring positions are determined by these maxima. However, as seen in Fig. 3, the pink-beam powder profile is strongly asymmetric so that the peak positions are offset to lower 2θ relative to the peak maxima. Moreover, the offset increases with increasing 2θ . This will bias the calibration routine to give a smaller sample–detector distance; in this case 87.73 mm was obtained rather than the design distance of 94 mm. The true distance is unknown but is between these two values. The image integration to produce the 1D powder pattern (Fig. 3) is affected by this bias so that the wavelength obtained in a Rietveld refinement (Table 1) using the known lattice parameters of NIST SRM674b (CeO₂, $a = 5.41153$ Å) is slightly less [$\lambda = 0.52015$ (4) Å] than the peak value in the energy profile (Fig. 1). Nonetheless, once calibrated against CeO₂, this wavelength can be used in analyses of sample data produced subsequently from the same sample wheel in LSS experiments at the DCS for determination of, for example, lattice parameters on the shock Hugoniot. It is important to recognize that this calibration would need to be performed after any change in the instrument configuration.

Of the coefficients defined in equations (7)–(10) above, only V , W , α_0 , β_0 and β_1 could be determined (Table 1); the other coefficients (U , X and α_1) were not required for obtaining a best fit to the data. They could become necessary with a different monochromator/slit configuration that yielded a sharper energy distribution.

In comparison with more conventional X-ray powder diffraction measurements, the peaks in this pink-beam experiment are much broader. This compromises the infor-

mation contained in the powder pattern. In this case the values obtained for the displacement parameters, $U_{\text{iso}}(\text{Ce}) = 0.0075$ (4) Å² and $U_{\text{iso}}(\text{O}) = 0.0166$ (14) Å², are much larger than expected for this material; changing them to more reasonable values (0.003 and 0.004, respectively) has little impact on the fit. Moreover, the broadening did not permit examination of the very small contribution from crystallite size or microstrain broadening anticipated for this sample. Use of a sharper energy distribution could help determine these values with more accuracy.

5. Conclusions

We have demonstrated here a suitable peak shape function for pink-beam powder diffraction patterns and employed it in the first application in a Rietveld refinement using a powder diffraction pattern accumulated in only 100 ps. It is anticipated that it will be useful in characterizing the evolution of simple materials in the extreme conditions available at the LSS station of the DCS at the Advanced Photon Source.

Funding information

Parts of this work were supported by LLNL under contract DE-AC52-07NA27344 and LDRD funding 18-ERD-012 and obtained at the Dynamic Compression Sector, which is operated by Washington State University under the US Department of Energy (DOE)/National Nuclear Security Administration award No. DE-NA0003957. This research used resources of the Advanced Photon Source, a DOE Office of Science User Facility operated for the DOE Office of Science by Argonne National Laboratory under contract No. DE-AC02-06CH11357.

References

- Bancroft, D., Peterson, E. L. & Minshall, S. (1956). *J. Appl. Phys.* **27**, 291–298.
- Briggs, R., Coppari, F., Gorman, M. G., Smith, R. F., Tracy, S. J., Coleman, A. L., Fernandez-Pañella, A., Millot, M., Eggert, J. H. & Fratanduono, D. E. (2019). *Phys. Rev. Lett.* **123**, 045701.
- Rietveld, H. M. (1969). *J. Appl. Cryst.* **2**, 65–71.
- Sharma, S. M., Turneaure, S. J., Winey, J. M. & Gupta, Y. M. (2020). *Phys. Rev. Lett.* **124**, 235701.
- Thompson, P., Cox, D. E. & Hastings, J. B. (1987). *J. Appl. Cryst.* **20**, 79–83.
- Toby, B. H. & Von Dreele, R. B. (2013). *J. Appl. Cryst.* **46**, 544–549.
- Von Dreele, R. B., Jorgensen, J. D. & Windsor, C. G. (1982). *J. Appl. Cryst.* **15**, 581–589.
- Wang, X., Rigg, P., Sethian, J., Sinclair, N., Weir, N., Williams, B., Zhang, J., Hawreliak, J., Toyoda, Y., Gupta, Y., Li, Y., Broege, D., Bromage, J., Earley, R., Guy, D. & Zuegel, J. (2019). *Rev. Sci. Instrum.* **90**, 053901.